Agriculture, Ecosystems and Environment 304 (2020) 107114

Contents lists available at ScienceDirect

Agriculture, Ecosystems and Environment

journal homepage: www.elsevier.com/locate/agee

Sediment sources, soil loss rates and sediment yields in a Karst plateau catchment in Southwest China

Qianyun Cheng[a,b], Shijie Wang[a], Tao Peng[a,d,*], Le Cao[a,b], Xinbao Zhang[c], Sarah J. Buckerfield[e,f], Yusheng Zhang[g], Adrian L. Collins[g]

[a] State Key Laboratory of Environment Geochemistry, Institute of Geochemistry, Chinese Academy of Sciences, Guiyang 550081, China
[b] University of Chinese Academy of Sciences, Beijing 100049, China
[c] Institute of Mountain Hazards and Environment, Chinese Academy of Sciences, Chengdu 610041, China
[d] Puding Karst Ecosystem Research Station, Chinese Academy of Sciences, Puding 562100, China
[e] Biological and Environmental Sciences, Faculty of Natural Sciences, University of Stirling, Stirling FJ9 4LA, UK
[f] Institute of Surface-Earth System Science, Tianjin University, Tianjin 300072, China
[g] Sustainable Agriculture Sciences Department, Rothamsted Research, North Wyke, Okehampton EX20 2SB, UK

ARTICLE INFO

Keywords:
Sediment source
Fingerprinting
^{137}Cs
Magnetic susceptibility
Karst
Headwater catchment
Critical zone

ABSTRACT

Intensive agricultural activities have accelerated soil erosion and rocky desertification in karst regions of southwest China. Knowledge of sediment sources and soil erosion rates can be used to target soil conservation measures and to improve calibration and validation of process-based soil erosion and sediment delivery models for scenario analyses. Due to the complexity of karst environments, however, catchment scale information on these components of sediment budgets has rarely been assembled, meaning there continues to be an evidence gap. Within this context, this study selected Chenqi catchment, given its appropriate research infrastructure, to investigate sediment sources and soil loss rates in a typical karst agroforestry landscape. We estimated the relative contributions from three sources: surface soil, subsurface soil and clastic rock, using a composite fingerprinting procedure combining ^{137}Cs and magnetic susceptibility and a frequentist un-mixing model with Monte Carlo uncertainty analysis. Suspended sediment samples were taken at an hourly interval during seven rainfall events in 2017–2018 to characterize and quantify the sediment exported in both surface and underground drainage. The overall average median contributions (with 5th-95th percentile uncertainty ranges) from the sources to the suspended sediment samples from the surface drainage outlet were in the order: 62% (0 – 99%) subsurface soils, 25% (0 – 91%) surface soils and 13% (0 – 45%) clastic rock. For the sediment samples collected from the underground drainage catchment outlet, the corresponding estimates were in the order: 68% (0 – 97%) subsurface soils, 25% (0 – 53%) clastic rock and 7% (0 – 44%) surface soils. Plot scale soil loss rates were highest on cropland (0.70 Mg km^{-2}) and pasture land (0.48 Mg km^{-2}). The average (2017 and 2018) annual suspended sediment load exported through the surface outlet was 4.64 Mg km^{-2} compared with 1.20 Mg km^{-2} through the underground outlet. The broader implications of this study are that subsurface and clastic rock sources represent a significant component of the catchment sediment budget, meaning erosion control measures targeting hillslope surface soils alone may have limited impact on suspended sediment export at landscape scale.

1. Introduction

Due to population pressure, the increasing intensity of human exploitation of the land has changed the landscape structure of karst areas and accelerated the speed of soil degradation, depletion of fertility, rocky desertification and reduction of biodiversity. This has resulted in the ongoing conflict between ecological protection and socio-economic development in karst areas (Hartmann et al., 2014; Cao et al., 2015; Li et al., 2017). Currently, rocky desertification caused by soil erosion in karst areas is highlighted as one serious ecological problem in southwest China, which not only restricts the sustainable development of the economy, but also directly threatens the ecological security of the Yangtze River and Pearl River basins (Peng and Wang, 2012; Jiang et al., 2014a; Martin et al., 2016; Dai et al., 2017). In karst environments, soils are often very thin and rocky, and channels in the underlying bedrock, apertures, and solution-enlarged fissures facilitate the

* Corresponding author at: State Key Laboratory of Environment Geochemistry, Institute of Geochemistry, Chinese Academy of Sciences, Guiyang 550081, China.
E-mail address: pengtao@mail.gyig.ac.cn (T. Peng).

https://doi.org/10.1016/j.agee.2020.107114
Received 13 May 2020; Received in revised form 8 July 2020; Accepted 2 August 2020
Available online 17 August 2020

transport of mobilized sediment from the land surface to underground systems. As a result, the lack of soil for cultivation severely threatens sustainable agriculture (Williams, 1983; White, 2007; Wilcox et al., 2007).

According to the 2018 national water and soil conservation bulletin, the total area of soil and water conservation measures in China was 9,916,196 km^2, whilst that in the eight karst provinces in southwest China was 3,302,593 km^2. Hillslope farmland, considered as the main source area of soil erosion, is currently the target for soil erosion protection measures since this source accounts for ~1/3 of the total soil erosion in China (Ministry of water resources, 2010). It is therefore considered to be of great importance to strengthen comprehensive control of soil loss on hillslope farmland, including in the karst regions of southwest China. However, sediment dynamics in karst regions are still unclear due to the extreme heterogeneity in the lithological and hydrological properties of well-developed karst. Understanding the provenance of suspended sediment exported from such catchments with various land use types can help understand how different agricultural activities and intrinsic landscape features and processes influence erosion rates and sediment source dynamics. Such information is needed to provide a more robust evidence base for selecting measures to control soil erosion, conserve soil and water resources, manage watersheds, and promote effective ecological restoration in karst areas.

Generally, soil migration downwards through pores and fissures into the joints and conduits which characterize karst aquifers and which provide rapid flow pathways, results in subsurface soil loss being an important soil erosion mechanism in karst landscapes (Yuan, 1997; Li et al., 2002; Zhang et al., 2007; Dai et al., 2015). However, the relative importance of surface soil erosion versus underground soil loss and indeed, in the context of additional sources, is still widely debated for the karst region in southwest China. Research on the ratio between surface and underground soil loss has still not resulted in consensus (Zhang et al., 2011; Zhou et al., 2012; Peng et al., 2013; Wei, 2013). Some researchers argue that underground soil loss is the main process of soil erosion (Jiang et al., 2014b; Li and Wu, 2015), while others suggest that surface soil loss is dominant because there is a greater volume of soil that can be eroded from farmed hillslopes rather than rock fissures (Wang et al., 2014; Wei et al., 2016). Besides, the lithology and landscape characteristics in karst catchments have recently been shown to have a strong influence on sediment yields, due to their effect on erosion mechanisms (Li et al., 2019). Karst catchments display a wide variation in lithology, from pure carbonate to carbonate highly intercalated with clastic rocks of varying solubility and erosivity. The higher concentration of insoluble components in non-carbonate rocks makes intercalated layers a possible intrinsic source of suspended sediments in karst areas, where the majority of carbonate rocks are highly soluble (Feng et al., 2014). However, this aspect of karst lithology, and the corresponding consequences for erosion and sediment source dynamics, has not been addressed; the easily erodible soils, rather than the insoluble clastic material have been the main focus of previous studies concerning the contributions of different sediment sources. Due to this heterogeneity and complexity in the erosivity of carbonates intercalated with clastic material, and the important role that clastic sediments plays in sediment transport and storage in karst landscapes (Bonacci, 1987), clastic rock pieces should be considered as one of the sediment sources and thus traditional measurement techniques may not be suitable for elucidating suspended sediment provenance, since these methods are not pragmatic for dealing with the often pronounced spatio-temporal variability of erosion and sediment delivery pathways.

Sediment fingerprinting has therefore been increasingly used as a tool for discriminating and apportioning sediment sources and erosion mechanisms in a range of geological and land use settings (Collins et al., 2010; Gellis and Walling, 2011; Miller et al., 2015; Owens et al., 2016; Collins et al., 2017). On this basis, fingerprinting methods may be a suitable approach to estimating sediment sources in karst catchments with dual-structure (i.e., surface and underground) drainage systems. Where such information can be integrated with measured sediment export, it is possible to quantify the magnitude of the net sediment loss from individual sources successfully discriminated by the source fingerprinting approach.

Fallout radionuclides and mineral magnetic properties are two types of tracer properties that have previously been used successfully to apportion sediment sources using the fingerprinting approach. ^{137}Cs ($t_{1/2}$ = 30.2 years) has been included in many studies as a fingerprint property to distinguish sediment sources associated with different depths (Russell et al., 2001; Matisoff et al., 2002; Nagle and Ritchie, 2004; He et al., 2009). The concentration of ^{137}Cs is independent of soil type and underlying geology, making it an appropriate source fingerprinting property in heterogeneous catchments such as those with karstic bedrock. Magnetic properties (namely magnetic susceptibility) can be particularly useful in constraining the origin of sediment, since the magnetic susceptibility of soils is linked to the degree of weathering and soil erosion (Gennadiev et al., 2002; Olson et al., 2002; Sadiki et al., 2009; Ayoubi et al., 2012; Rahimi et al., 2013; Jordanova et al., 2014). It was therefore deemed logical to test these properties in applying the source fingerprinting approach in a typical karst catchment. More specifically, the objectives of this study were: (i) to identify the principal sources of the suspended sediment exported from a typical agroforestry karst catchment in southwest China using catchment-specific composite source fingerprinting including an un-mixing model with uncertainty analysis, and; (ii) to integrate the source fingerprinting estimates with measurements of sediment export to quantify the magnitude of net sediment loss from individual sources, and (iii) to describe how agricultural activities influence the soil erosion processes in karst areas.

2. Materials and methods

2.1. Study area

The study area, Chenqi catchment (1.3 km^2; 26°15′36″N, 105°43′30″E), is located in Puding County, Guizhou Province, southwest China. It is part of the Wujiang River catchment of the Yangtze River basin (Fig. 1). Chenqi has an altitude range of 1316 m–1500 m a.s.l. The region has a subtropical monsoonal climate with an annual mean temperature of 14 ℃ and total precipitation of 1336 mm. The temperature ranges from an average minimum of -1 ℃ to an average maximum of 28 ℃, and over 80 % of the rain in any year falls between May and October. The study area is a typical karst agroforestry catchment of the central Guizhou plateau, containing a range of karstic landforms, including karst gullies, dry valleys and small karst caves. The valley depression with a thick soil profile is used for paddy cultivation, whereas the gentle hillslopes are used for the cultivation of other crops. Steeply sloping hillslopes are partially grazed but were also partially re-forested in conjunction with land conversion under the 'Grain for Green' project in the 1990s (Jintao, 2004).

The lithology is mainly thick bioclastic limestone strata of the Middle Triassic Guanling Formation with thin interbeds of muddy limestone (Fig. 2). Clastic rock pieces are contained within silicate interbeds and the carbonate strata. The primary drainage networks for the surface and underground catchments are spatially very similar. A surface river that has been fully contained within concrete channeling runs from the eastern slopes through the valley depression to the outlet in the west, receiving discharge from numerous gullies draining the hillslopes. The primary groundwater channel follows a similar geometry. The underground outlet is a rising spring at the mudstone aquitard layer, and the surface outlet is an ephemeral stream. A hydrological station at the catchment outlet measures discharge at a 5-minute interval from both the underground and surface water outlets. There are six bounded runoff fields distributed on the slopes of the study catchment (Fig.1), representing different land uses including the recovered land after burning (BAR), the non-recovered land after

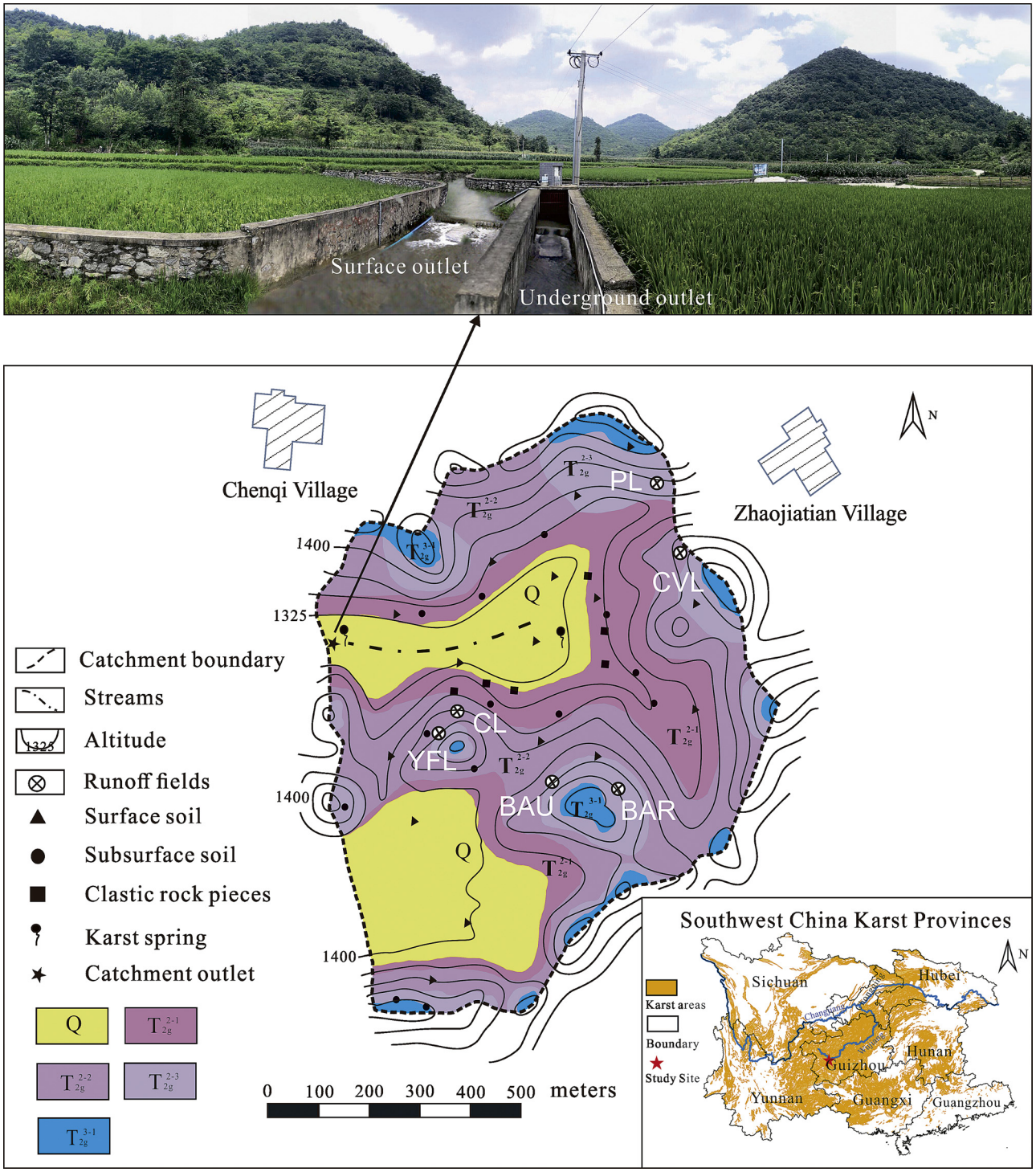

Fig. 1. Location of the karst study catchment and a photo of the surface and underground hydrological outlets.

burning (BAU), combined vegetation land (CVL), continued cropland (CL), young forestland (YFL), and pastureland (PL) (Peng and Wang, 2012).

2.2. Soil and sediment sampling

Three potential sediment sources were sampled during the dry season from December 2016 to April 2017, yielding 16 surface soil samples from hillslopes, 13 subsurface soil samples and six clastic rock samples. The distribution of the source samples is shown in Fig. 1. The surface soil was collected from a depth of 0 – 5 cm in areas with four types of land use comprising forest, pastureland, slope cropland, and paddy fields. Each sample was a composite of five subsamples collected from a two-meter radius of the sampling point using a wooden shovel. The subsurface soil samples were collected from eroding gully banks and from rock fissures. Three subsamples with different depths (excluding the topsoil part) from the gully banks or the fissures were composited in each subsurface soil sample. The clastic rock pieces were collected from slopes where the interbedded mudstone layers outcrop. Undissolved clastic rock was included as a potential sediment source following published reviews for karst systems (Herman et al., 2012; Herman, 2012; Hartmann et al., 2014).

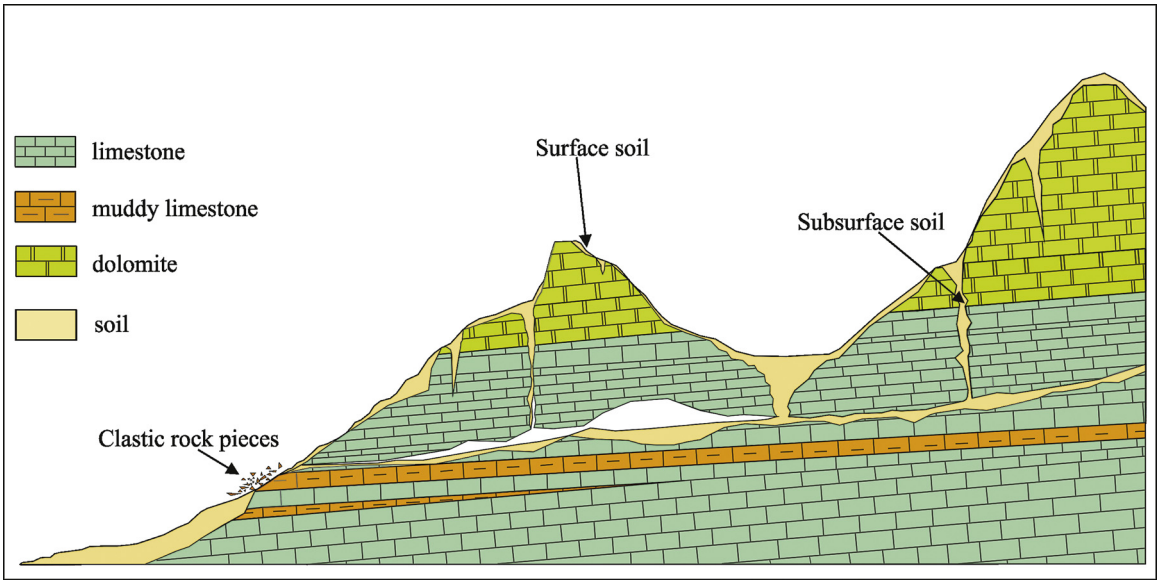

Fig. 2. Schematic showing the three principal sediment source types in the study catchment geological profile.

Suspended sediment samples were collected from the surface and underground outlets during seven heavy rainfall events in the wet seasons of 2017 and 2018. In 2017, we found that hourly samples did not yield sufficient sediment mass for ^{137}Cs analysis. Thus, to retrieve sufficient sample mass, bulk (200 L) water samples were collected with a large bucket every 30 ~ 60 min during the storms sampled in 2018. For those sediment samples with less mass collected in 2017, samples from two runoff events with similar rainfall characteristics were bulked to permit laboratory analysis of this particular sediment tracer.

2.3. Laboratory analyses

A Beckman Coulter LS3320 laser diffraction particle analyzer was used to measure the particle size of suspended sediment samples. Before the test, 10 % H_2O_2 was added, according to the sample volume and sediment concentration, to remove the organic matter in the sample. Here, the solution was heated to boiling point, then the carbonate was removed by adding 10 % HCl. Finally, 0.25 mol/L $Na_2P_2O_7$ was added for full dispersion of the sediment sample. The results of the laser diffraction particle size analysis were used to select the most appropriate mesh size (63 μm) for sieving the samples collected in the study catchment to assist direct comparisons of tracer contents.

Source material samples were dry-sieved to < 63 μm while suspended sediments were wet-sieved to < 63 μm and oven dried at 45℃. Analyses for ^{137}Cs and magnetic susceptibility were undertaken only on the sieved (< 63 μm) particle size fraction of the source material and suspended sediment samples. Since the source and suspended sediment samples were sieved to the same specific particle size fraction, an additional correction factor (e.g., (He and Walling, 1996)) for selectivity during erosion and sediment delivery was not utilized.

^{137}Cs activities in the source material and sediment samples were measured using a gamma-ray spectrometer and detected at 662 keV. Count times for each sample exceeded 33,000 s, providing results with an analytical precision of approximately ± 5% at the 90 % level of confidence. The magnetic susceptibility of the source material and suspended sediment samples was measured by using a Bartington MS2B dual-frequency magnetization meter (low frequency 470 Hz, high frequency 4700 Hz). Here, we focused on measuring the low frequency mass-specific magnetic susceptibility, since this provided a composite measurement of the total magnetic and non-magnetic constituents with each sample, providing results with an analytical precision up to 0.1 × 10^{-5} SI and a relative error of 1%.

2.4. Sediment source discrimination and ascription

With respect to data processing, the two key stages concern source discrimination, followed by source apportionment. Prior knowledge of tracer behaviour is helpful when considering the most appropriate tracer for a given environmental setting (Collins et al., 2017). Tracers with small differences between source groups should be rejected as they generate larger uncertainties in the estimated source proportions than tracers with greater between-group contrasts (Collins and Walling, 2002). Additionally, tracers used in composite fingerprints should show conservative behaviour during mobilization and delivery through the study catchment. This can be tested using biplots of tracer pairings which is considered to provide a more sensitive test for tracer conservatism (Pulley and Collins, 2018; Nosrati and Collins, 2019) than the conventional range or bracket test (Foster and Lees, 1999).

The frequentist numerical mass balance model of Collins et al. (2010a) was used to calculate the relative contributions from each source, by using the function in Eq.1:

$$\mathrm{RSS}=\sum_{i=1}^{n}\left\{\left[C_{ssi}-\left(\sum_{s=1}^{m}P_sC_{si}\right)\right]/C_{ssi}\right\}^2 W_i \quad (1)$$

where: C_{ssi} = deviate median concentration of fingerprint property (i) in target surface or subsurface sediment samples; P_s = the optimized percentage contribution from source category (s); C_{si} = deviate median concentration of fingerprint property (i) in source category (s); W_i = the tracer discriminatory power weighting.

Uncertainty ranges for the predicted source proportions were determined using a Monte Carlo sampling routine (Collins et al., 2012; Theuring et al., 2015). Here, the model input probability density functions representing the tracer values in the source categories were constructed using the mean and Qn (Rousseeuw and Croux, 1993) for each tracer. Similarly, probability density functions were constructed in the same manner to represent the tracer values in either the surface or subsurface target sediment samples. The mixing model was run until 5000 iterations satisfied a threshold for absolute mixing model error of ≤20 %. One batch run was undertaken for the surface sediment samples, and another for the subsurface sediment samples.

To evaluate the predicted source proportions for either the surface or subsurface sediment samples, virtual mixture tests were performed since this is now established as a standard, but important, methodological step in source fingerprinting studies (Palazón et al., 2015; Collins

Table 1
Sample numbers analyzed (n) and summary data for all tracers.

	n	^{137}Cs (Bq kg^{-1})		χlf (10^{-8} m^3 kg^{-1})		χhf (10^{-8} m^3 kg^{-1})		Xfd (%)	
		Mean	CV (%)	Mean	CV (%)	Mean	CV (%)	Mean	CV (%)
Surface soil	16	3.39	21	310.07	13	280.82	14	9.47	16
Subsurface soil	13	0.50	10	180.69	11	162.22	11	10.23	19
Clastic rock pieces	6	0	–	7.02	12	6.82	12	2.72	116
Suspended sediments	10	2.92	57	134.36	31	119.47	31	11.20	8

CV: Coefficient of variation.

et al., 2017; Pulley and Collins, 2018; Nosrati and Collins, 2019). More specifically, 20 virtual mixtures were generated with different proportions of the three sources under scrutiny. The proportions were 0.05, 0.15, 0.3, 0.5, 0.7, 0.85 and 0.95 and a stratified sampling approach was employed whereby one source was assigned a specified value from this list and the remaining two sources were assigned equal shares of the remaining proportion. For example, one virtual mixture could have a specified proportion of 0.3 for one source, with the other two sources assigned the same proportion (0.35 each) in order to meet the underpinning mixing model assumption that all source contributions should sum to unity. The Qn values of the tracer properties were assumed to be same as the Qn values estimated for either all the surface or subsurface sediment samples. Scatter plots of the actual known source proportions and the predicted proportions for the three sources were plotted for comparison and assessment of the mixing model accuracy.

2.5. Measuring hillslope runoff

Surface runoff and soil loss on the study catchment hillslopes with different land use were monitored using the large bounded runoff field method. Since the hillslope area accounts for 75 % of the total area of the study catchment, monitoring the runoff and soil erosion of these fields was assumed to provide a reasonable approximation of surface soil erosion in the study catchment. More specifically, runoff and mobilized sediment were collected in sedimentation tanks during storm events (see locations in Fig. 1). Each tank was coupled to a square shaped collection pond (Peng and Wang, 2012). The runoff in the square pools was designed to represent one-eighth of the total runoff generated on the fields (based on surface area). The volume of the runoff in the tanks and square pools was measured after each rainfall event, and a 500 ml sample was retrieved from each of the square pools after stirring and mixing of the collected water-sediment mix, to provide an estimate of the sediment concentration in the hillslope runoff. The soil erosion on hillslopes associated with each rainfall event could thus be obtained. Additionally, the mobilized material reaching the tanks and pools was retrieved, filtered and weighed in case of the need for further geochemical analysis. The total erosion loss was calculated by adding the results for every sampled rainfall event.

2.6. Discharge and sediment load monitoring at the study catchment outlet

The turbidity in the surface and underground catchment outlets was monitored, in situ, at a 10-minute interval using a VisoTurb@700IQ online turbidity analyzer manufactured by WTW (NTU range 0–300; NTU precision 0.1). The rating relationship between turbidity and gravimetrically-filtered suspended sediment concentration was derived and the overall suspended sediment yield calculated using the following empirical Eq. (2):

$$M = \frac{1}{1000}\sum_{i-1}^{n}(aX + b) \times Q \times T \quad (2)$$

where: M = suspended sediment load, kg; n = frequency; a = slope coefficient in the rating equation; X = turbidity, NTU; b = intercept coefficient in the rating equation; Q = flow rate, m^3/s; T = time resolution, s.

3. Results

3.1. Sample characteristics and rainfall event data

The suspended sediment samples from the surface and subsurface water outlets showed that the < 63 μm particle size fraction constituted over 85% of the suspended sediment samples collected in both the surface and subsurface flows (Table 2). Using the < 63 μm particle size fraction was thus considered reasonable for the objective of this study.

The concentrations of ^{137}Cs and the magnetic susceptibility of the three source types are shown in Table 1. In the case of the surface soil samples, there was no significant difference in either the ^{137}Cs or magnetic susceptibility among the different land uses (Table 3). ^{137}Cs values in the sampled surface soils were highest, ranging from 2.28 to 4.77 Bq/kg, with a corresponding average of 3.39 Bq/kg, because ^{137}Cs is enriched in surface soils due to fallout associated with atmospheric weapons testing during the 1950 s–1970 s. In contrast, the subsurface soil samples had low values of ^{137}Cs, ranging from 0.00 to 0.65 Bq/kg with a corresponding average value of 0.50 Bq/kg, because subsurface soils are either beneath surface soils in gully walls or deeply buried in karst fissures and thereby receive less atmospheric fallout. There was no detectable ^{137}Cs in the clastic rock pieces (Table 1) because this material has had no exposure to the atmospheric fallout.

Unlike ^{137}Cs, the magnetic susceptibility of soil is a comprehensive reflection of soil forming factors and processes. The surface soil, subsurface soil and clastic rock pieces have experienced different environmental transformation. Accordingly, the magnetic susceptibility data can provide useful information for source discrimination and apportionment. The surface soil had high magnetic susceptibility (Table 1), ranging between 205.11·10^{-8} m^3/kg and 370.13·10^{-8} m^3/kg, with a corresponding average of 310.07·10^{-8} m^3/kg. The magnetic

Table 2
The proportion of suspended sediment samples comprised by the < 63 μm particle size fraction.

Suspended sediment sample	Percentage < 63μm
2017[s]	97.07
2017[u]	96.38
2018/ 05/27[s]	100
2018/06/02[s]	92.57
2018/06/20[s]	100
2018/06/20[u]	99.57
2018/08/08[s]	93.94
2018/08/08[u]	95.08
2018/08/22[s]	93.94
2018/08/22[u]	88.28

[s] refers to suspended sediment samples collected from the surface outlet.
[u] refers to suspended sediment samples collected from the underground outlet; note samples collected to represent storm events in 2017 were the composites of material collected in three successive storms.

Table 3
Summary tracer characteristics of the surface soil samples collected from four land-use types and suspended sediment samples.

	N	^{137}Cs (Bq kg^{-1})			χlf (10^{-8} m^3 kg^{-1})			χhf (10^{-8} m^3 kg^{-1})			Xfd(%)		
		Mean	Min	Max	Mean	Min	Max	Mean	Min	Max	Mean	Min	Max
Forest	4	3.97	2.40	4.77	308.00	255.56	353.92	281.19	232.86	322.50	8.80	6.53	10.90
Pastureland	4	3.41	2.78	3.77	276.73	205.11	323.59	246.98	185.40	286.44	10.65	9.61	11.48
Paddy	4	3.21	3.01	3.72	331.52	298.12	370.13	300.85	267.16	345.11	9.37	6.76	10.96
Sloping cultivated land	4	2.96	2.28	4.01	324.04	290.29	355.80	294.67	260.60	319.22	9.07	7.82	10.28
Suspended sediment	10	2.92	0.54	4.95	134.36	63.59	188.80	119.47	55.30	167.22	11.20	10.12	13.04

Summary tracer characteristics of the surface soil samples collected from four land-use types and suspended sediment samples.

susceptibility of subsurface soil (Table 1) was slightly lower, ranging from 145.28·10^{-8} m^3/kg to 198.50·10^{-8} m^3/kg, with an average value of 180.69·10^{-8} m^3/kg. The magnetic susceptibility of clastic rock pieces was extremely low, ranging between 5.50·10^{-8} m^3/kg and 7.90·10^{-8} m^3/kg, with an average of 7.02·10^{-8} m^3/kg. The magnetic susceptibility of the samples collected in the study area was consistent with the magnetic parameters of the soil profiles of carbonate rocks in Guizhou province published by previous studies (Lu, 2003). Here, the higher magnetic susceptibility of the surface soil is likely to be due to a high degree of weathering, with the subsurface soil having a lower magnetic susceptibility than the surface soil, and the basement carbonate rock having the lowest magnetic susceptibility. Overall, the magnetic susceptibility data for the three sources indicates that this tracer is closely related to weathering intensity and the soil forming environment.

Table 4 presents summary data for the rainfall events sampled during this study. The highest rainfall event total precipitation was 50.2 mm. The maximum I_{30} was 39.2 mm h^{-1}. The total kinetic energy calculated for the individual rainfall events ranged between 3.71 and 9.69 J m^{-2}. The rainfall erosivity ranged between 29.76 and 193.80 J mm m^{-2} h^{-1}.

3.2. Sediment source discrimination and apportionment

The Kruskal-Wallis H-test indicated that both ^{137}Cs and magnetic susceptibility were significantly different ($p < 0.05$) among surface soil, subsurface soil and clastic rock samples (Table 5). The results in Table 6 confirm that our composite fingerprint correctly classified 100 % of the source samples. Biplots of tracer pairings (Fig. 3) showed that magnetic susceptibilities with both high and low frequency were conservative since all samples plot along the same line, whilst ^{137}Cs and mineral magnetic properties plot within the same space, again indicating conservative behaviour.

The estimated average median relative contributions (with corresponding 5th – 95th percentile ranges) from the three source types to the catchment surface and underground sampled suspended sediment loads are presented in Table 7. The overall average median contributions from the catchment sources to the suspended sediment samples collected in the surface drainage outlet were estimated at: 62 % (0 – 99%) subsurface soils, 25 % (0 – 91%) surface soils and 13 % (0 – 45%) clastic rock. For the sediment samples collected in the underground drainage catchment outlet, the corresponding estimates were estimated to be: 68 % (0 – 97%) subsurface soils, 25 % (0 – 53%) clastic rock and 7% (0 – 44%) surface soils. For both, the surface and underground drainage outlets, the subsurface soils were therefore identified as the dominant suspended sediment source during the 2017–2018 study period. Eroding surface soils were identified as being a more important source of the suspended sediment samples collected from the surface drainage pathway, rather than the underground catchment outlet. Source fingerprinting suggested that clastic rock contributions were higher for the suspended sediment samples collected from the underground drainage pathway.

Fig. 4 summarizes the results of the virtual mixture tests comparing known and predicted contributions from the individual sources. These results show that the un-mixing model performed best for the surface soil (errors up to ~15 %) and clastic rock (errors up to ~5%) sources and least well for the subsurface source category (errors up to ~19 %).

Table 4
Summary data for the rainfall events sampled by this study.

Date		P (mm)	I_{30} (mm h^{-1})	Period (h)	I_{mean} (mm h^{-1})	E(J m^{-2})	R(J mm m^{-2} h^{-1})
2017	06/15	26.2	6.0	9.0	2.9	4.96	29.76
	06/30	50.2	12.0	16.0	3.1	4.09	49.08
2018	05/27	32.8	14.4	9.6	3.4	4.94	71.14
	06/02	28.6	12.4	13.5	2.1	3.71	46.00
	06/20	50.2	20.0	10.8	4.7	9.69	193.80
	08/08	32.6	19.4	16.7	2.0	4.62	89.63
	08/22	24.8	39.2	3.3	7.4	5.10	199.92

P: precipitation; I_{30}: maximum rainfall intensity in 30 min; Period: duration (hours) of the rainfall event; I_{mean}: average rainfall intensity; E: total kinetic energy; R: rainfall erosivity.

Table 5
The results of the Kruskal-Wallis H-test for the sediment source discriminatory power of the tracer properties.

Property	H-value	*p*-value
^{137}Cs	28.227	0.000*
χlf	28.862	0.000*
χhf	28.862	0.000*
χfd	13.141	0.001*

* significantly different at $p < 0.05$ significance level.

Table 6
Discriminatory efficiency of the composite signature.

Property	%[1]	TDW[2]
^{137}Cs	82.9	1.53
χlf	97.1	1.79
χhf	97.1	1.79
χfd	54.3	1.00
Total[3]	100	

[1] % source samples classified correctly by individual tracers.
[2] tracer discriminatory weighting used in the frequentist model for source apportionment.
[3] source samples classified correctly by composite signature.

3.3. Annual surface soil loss from different land uses and the catchment suspended sediment yields

Table 8 shows the estimated soil loss for the six types of land use on the karst hillslopes measured in 2017 and 2018. The CL and PL had the greatest soil loss rates, followed by the BAR, with the BAU and CVL having no measured soil loss. We calculated the annual sediment loads from the outlets for the water years 2017 and 2018. The annual

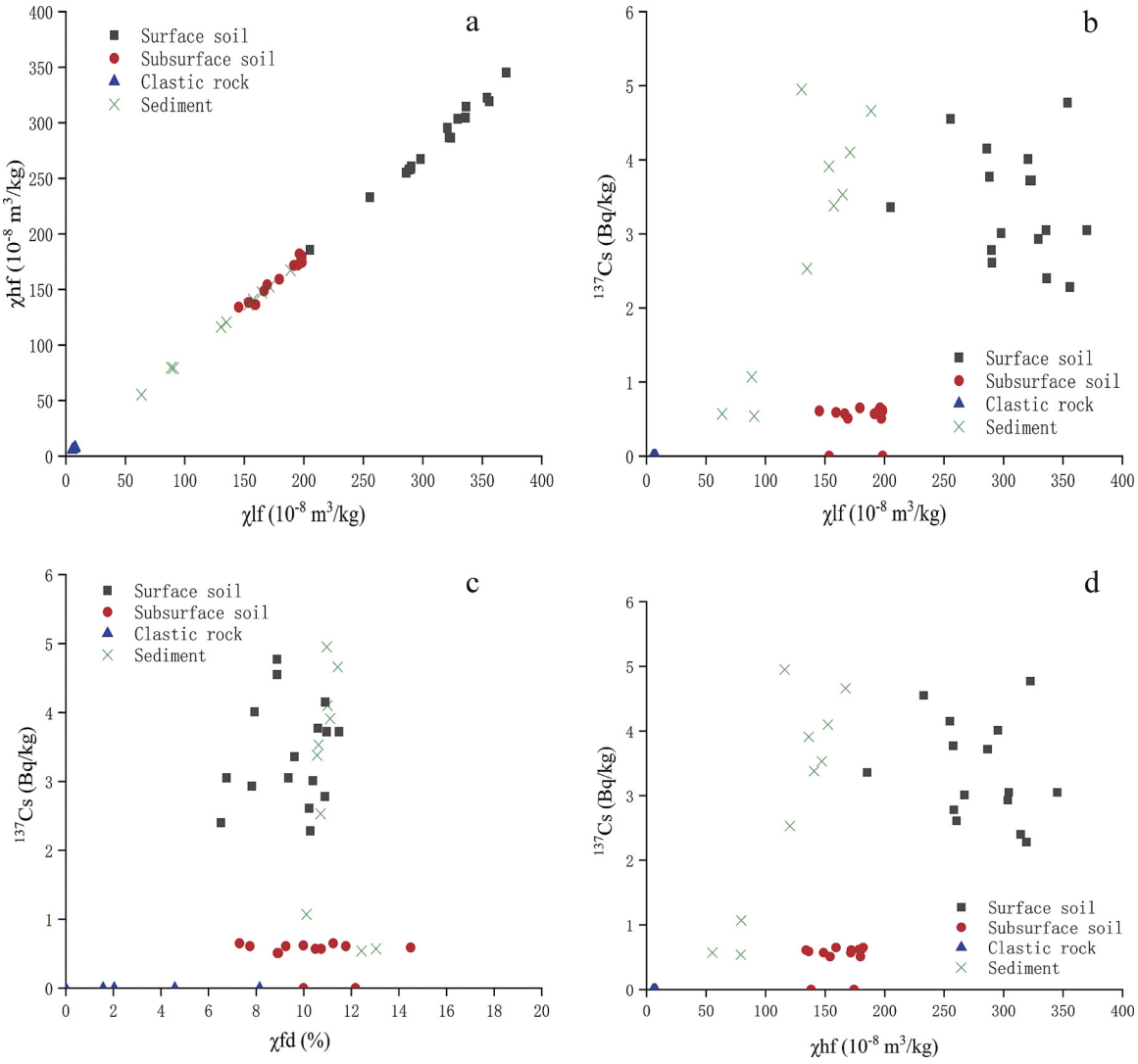

Fig. 3. Biplots of tracer pairings for source and suspended samples.

Table 7
Average median (with Monte Carlo full uncertainty ranges in brackets) relative contributions (%) from surface soil, subsurface soil and clastic rock to suspended sediment sampled in the surface and underground water outlets of the Chenqi study catchment during 2017 and 2018.

	Surface soil	Subsurface soil	Clastic rock
Surface outlet	25 (0 – 91)	62 (0 – 99)	13 (0 – 45)
Underground outlet	7 (0 – 44)	68 (0 – 97)	25 (0 – 53)

Table 8
Annual soil loss on karst slopes under different land use (2017-2018).

Year	Annual soil loss (Mg km^{-2} year^{-1})					
	BAR	BAU	CL	PL	YFL	CVL
2017	0.21	0	0.86	0.73	0	0
2018	0.05	0	0.53	0.23	0	0
Mean	0.13	0	0.70	0.48	0	0

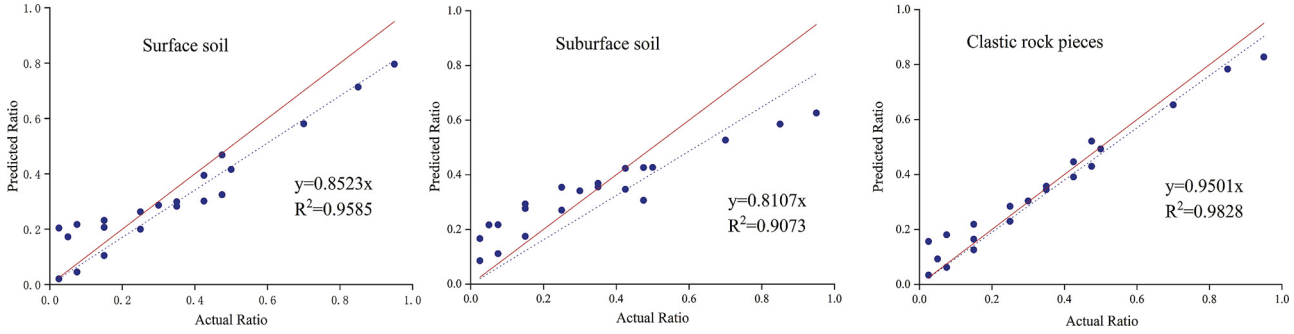

Fig. 4. Visual test results comparing known and predicted contributions.

sediment loads from the surface outlet were calculated to be 4.08 Mg/km^2 and 5.19 Mg/km^2 in 2017 and 2018, respectively. The corresponding annual sediment loads exported along the underground pathway were 1.00 Mg/km^2 and 1.40 Mg/km^2 in 2017 and 2018, respectively. Combined with the estimated source proportions (Table 7), in the case of the surface outlet, the total net sediment loss from eroding subsurface soils during the two sampling years was 5.75 Mg/km^2 (2.53 Mg/km^2 in 2017 and 3.22 Mg/km^2 in 2018). The corresponding estimate for surface soils was 2.32 Mg/km^2 (1.02 Mg/km^2 in 2017 and 1.30 Mg/km^2 in 2018). In the case of the clastic rock sediment source, the corresponding estimate was 1.2 Mg/km^2 (0.53 Mg/km^2 in 2017 and 0.67 Mg/km^2 in 2018). For the underground sediment export pathway, the corresponding estimates were 1.63 Mg/km^2 (0.68 Mg/km^2 in 2017 and 0.95 Mg/km^2 in 2018) from eroded subsurface soils, 0.17 Mg/km^2 (0.07 Mg/km^2 in 2017 and 0.10 Mg/km^2 in 2018) from eroded surface soils, and 0.6 Mg/km^2 (0.25 Mg/km^2 in 2017 and 0.35 Mg/km^2 in 2018) from clastic rocks.

4. Discussion

4.1. Soil erosion features and sediment sources in the karst agroforestry catchment system

Our study indicates that the combination of the underlying geological strata and overlying land-use, is the first order control on soil erosion and sediment source. The subsurface soil source contributed most of the sampled suspended sediments. More than half of the material sampled in both the surface flow and from the underground outlet were predicted to come from the subsurface sources. The subsurface soil source consists of two primary components; soil in the underground system and material eroded from gully or river banks. Field observations suggested that the mobilization of subsurface soil from gully/channel wall erosion during floods is important, especially in the case of the subsurface soil contribution to the suspended sediment samples collected in the surface drainage outlet. In contrast, the main contribution of the subsurface source to the underground outlet sediment samples is more likely to be the result of soil from rock fissures delivered into the underground river system through the dissolving fissures; an underground leakage process unique to karst landscapes. Gully erosion in small catchments is often characterized by deep sidewalls and steep profiles, and can be an important suspended sediment contributor (Poesen et al., 2003; Mararakanye and Sumner, 2017). For example, it has been estimated that gully erosion could contribute 60%–90% of the total sediment yield in the hilly region of the Chinese Loess Plateau (Wang et al., 2003; Ni et al., 2017). Surface runoff in karst constitutes a minor proportion of total rainwater flux. Instead, most of the rainwater seeps down into the underground fissured structures through the porous lithology. Flushing of underground soils thus occurs when there is high-intensity runoff moving quickly downwards through cracks and fissures during rainfall events, accounting for most of the sampled suspended sediment in our karst catchment. Such pathways and source contributions are highly likely to be more generally representative of the karst catchments in southwestern China.

Surface soils consistently contributed less to the suspended sediment samples. The surface soils from both hillslopes and paddy land contributed little to the sampled suspended sediment collected in the surface outlet because there was limited surface runoff on the hillslopes and where it was observed, it only transported detached soil short distances during rain storms. Other studies (Chen et al., 2008; Peng et al., 2008, 2011; Chen et al., 2012; Zhang et al., 2014) have reported that surface runoff processes are insignificant for soil erosion in karst landscapes, and that underground erosion, remobilization, and underground runoff are, instead, the main processes responsible for sediment transport in karst terrain. This is not an unexpected result considering that subsurface pore space and fissures provide pathways for runoff, resulting in high permeability at the land surface in karst landscapes (Fu et al., 2015). Due to the limited surface runoff, limited sediment transport can occur on slope surfaces, which results in a lower contribution (relative to subsurface soils) to sampled suspended sediments at this headwater catchment scale.

The clastic rock outcrops were the least significant suspended sediment source for both the surface and underground hydrological outlets. Mudstone interbedded with the carbonate strata in the middle section of the Guanling Formation forms impermeable layers in our study catchment, preventing infiltration of fracture-hosted water. When large volumes of precipitation infiltrate the epikarst during heavy rainfall events in the wet season, the mudstone aquitard layers block infiltration and cause horizontal flow and water emergence at epikarst springs (Bonacci, 1987). As a result, erosion occurs at the mudstone-carbonate interface and muddy intercalated debris is transported to the river system. By way of comparison, albeit on a different lithology, previous work in the Huangfuchuan catchment on the northern Loess Plateau, has estimated the contribution from easily eroded coarse sandstone (the Pisha sandstone) which constitutes a small fraction of the local lithological strata. In this case, it contributed more than half of the dam infill sediment deposits associated with 31 rainfall events over the period 1958–1972 (Zhao et al., 2015, 2017). Regardless of the contrasts in the significance of clastic layers in karst or sandstone regions, our estimated contributions from clastic rocks illustrates that suspended sediment sources in karst catchments in southwestern China are influenced by the composition of the geological strata.

4.2. Historical agricultural activity and rainfall as controls on present day sediment sources and yields

An interesting dimension to the interpretation of our findings concerns the issue of legacy sediment mobilized from surface sources in the past. Between 1979–1981, farmers cleared trees without restriction in some areas due to the adjustment of rural land use rights, which resulted in severe soil erosion on sloping fields by surface runoff. Deforestation to expand available farm land often triggered severe soil erosion in the Guizhou karst plateau region due to high population pressure, and it has been estimated that erosion rates on hillslopes could potentially have reached thousands of tones per square kilometer every year after the period of deforestation and ensuing cultivation. Here, for instance, a large amount of soil was eroded during the 1980s in southwest China (Lin and Zhu, 1999; Zhang et al., 2011). In addition, ^{137}Cs concentrations measured in the soils of karst depressions (Zhang et al., 2009) and in the sediment deposits of reservoirs (Wan et al., 1991; Wenbo et al., 2008; Zhang et al., 2009) indicate that the soil eroded during the 1980s was very high in ^{137}Cs content. Research in karst depressions near Chenqi catchment have also reported that, in 2007, the peak concentration of ^{137}Cs could be as high as 7.25 Bq/kg in 2007 (Zhang et al., 2010), which would have diminished to 5.63 Bq/kg in 2018 based on known radionuclide decay rates. Following the same theory, the average concentration of ^{137}Cs from the field runoff sediments in the Chenqi study catchment in 2007 was 6.80 Bq/kg (Bai et al., 2009), which would diminish to 5.28 Bq/kg in 2018. When the rainfall erosivity exceeded a certain point, 49.08 J mm m^{-2} h^{-1}, sediments stored in large volume subterranean cavity spaces in karst can be remobilized out of the subsurface structure and contribute as a source to suspended sediment sampled in the present day (i.e., our study period). The old sediment eroded from the surface soils during and after deforestation several decades ago is hence a contributor to the suspended sediment exported from the catchment during contemporary heavy rainfall events. Fig. 5 shows a schematic of how the historical soil erosion pathways (Fig. 5a) changed following deforestation and ensuing cultivation during the 1980s (Fig. 5b). Soil erosion during the years immediately following deforestation and ensuing cultivation in our karst catchment mean that subsurface source contributions from rock fissures now release legacy sediments during those rainstorms capable of flushing subterranean stores. Measures to protect soil from

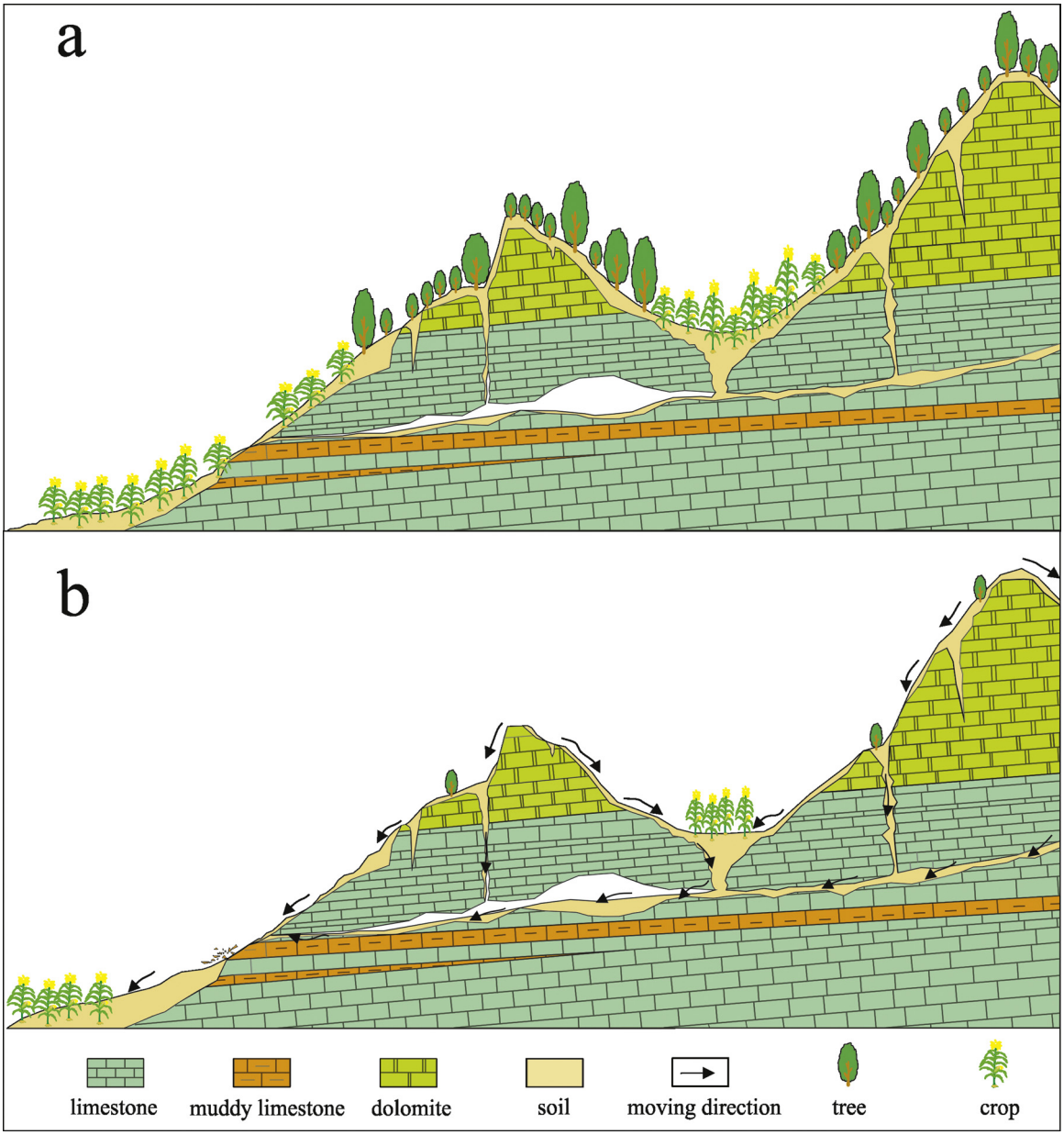

Fig. 5. A schematic of how the historical soil erosion pathways changed.

erosion should be focused on the early years after deforestation for hillslope farming. Where mitigation measures are not implemented with sufficient timeliness, the movement of surface soil into underground rock fissures generates a secondary source of legacy sediment which continues to be remobilized in the present day, helping to account for the importance of subsurface sediment sources, alongside the erosion of gully walls. An accurate threshold value to determine the risk of remobilization of legacy sediment sequestered in underground structures such as fissures could be identified through monitoring more rainfall events.

5. Conclusion

Rainfall characteristics, historical agricultural activity, bedrock lithology, and the dual-structure of the karstic drainage system are all important controls on suspended sediment dynamics in karst watersheds. Lithology is a strong control on sediment composition and the underground drainage structure provides efficient pathways for sediment remobilization and transport. Measures for soil erosion prevention should be focused on areas with deforestation and ensuing cultivation, as well as outcropping areas of intercalated clastic rock. Nevertheless, further work is required to apply source fingerprinting at larger catchment scales in the karst to assess scale dependency in sediment dynamics resulting from the interactions between lithology, land use and best management programmes.

Declaration of Competing Interest

We declared that we have no conflicts of interest to this work. We declare that we do not have any commercial or associative interest that represents a conflict of interest in connection with the work submitted.

Acknowledgements

The work was supported by the National Key Research and Development Program of China [2016YFC0502602]; the National Natural Science Foundation of China [41571130074, U1612441,

41403112]; the International Partnership Project [132852KYSB20170029]; and Guizhou Provincial Science and Technology Department Project [(2018)5405]. Huai Su (Yunnan Normal University) and Runchuan Zhang (Institute of Mountain Hazards and Environment) offered help with the laboratory analyses for ^{137}Cs and magnetic susceptibility. The contribution of YZ and ALC to this paper was supported by funding from UK Research and Innovation (UKRI) via the Soil to Nutrition institute strategic programme grant (BBS/E/C/000I0330) from the UKRI-Biotechnology and Biological Sciences Research Council (UKRI-BBSRC).

References

Ayoubi, S., Ahmadi, M., Abdi, M.R., Afshar, F.A., 2012. Relationships of Cs-137 inventory with magnetic measures of calcareous soils of hilly region in Iran. J. Environ. Radioact. 112, 45–51.
Bai, X., Zhang, X., Wang, S., Yan, D., Lihao, 2009. Estimating sediment deposition rates by the Cs-137 technique in karst depression of Chongtou, Puding County,Guizhou Province. Earth and Environment 37, 142–146.
Bonacci, O., 1987. Karst Springs. In: Bonacci, O. (Ed.), Karst Hydrology: With Special Reference to the Dinaric Karst. Springer, Berlin Heidelberg, Berlin, Heidelberg, pp. 49–102.
Cao, J., Yuan, D., Tong, L., Mallik, A., Yang, H., Huang, F., 2015. An overview of karst ecosystem in Southwest China: current state and future management. J. Resour. Ecol. 6, 247–256.
Chen, X., Chen, C., Hao, Q., Zhang, Z., Shi, P., 2008. Simulation of rainfall-underground outflow responses of a karstic watershed in Southwest China with an artificial neural network. Water Sci. Eng. 1, 1–9.
Chen, H., Liu, J., Zhang, W., Wang, K., 2012. Soil hydraulic properties on the steep karst hillslopes in northwest Guangxi, China. Environ. Earth Sci. 66, 371–379.
Collins, A.L., Walling, D.E., 2002. Selecting fingerprint properties for discriminating potential suspended sediment sources in river basins. J. Hydrol. (Amst) 261, 218–244.
Collins, A.L., Walling, D.E., Webb, L., King, P., 2010. Apportioning catchment scale sediment sources using a modified composite fingerprinting technique incorporating property weightings and prior information. Geoderma 155, 249–261.
Collins, A.L., Zhang, Y., McChesney, D., Walling, D.E., Haley, S.M., Smith, P., 2012. Sediment source tracing in a lowland agricultural catchment in southern England using a modified procedure combining statistical analysis and numerical modelling. Sci. Total Environ. 414, 301–317.
Collins, A.L., Pulley, S., Foster, I.D., Gellis, A., Porto, P., Horowitz, A.J., 2017. Sediment source fingerprinting as an aid to catchment management: a review of the current state of knowledge and a methodological decision-tree for end-users. J. Environ. Manage. 194, 86–108.
Dai, Q., Liu, Z., Shao, H., Yang, Z., 2015. Karst bare slope soil erosion and soil quality: a simulation case study. Solid Earth 6, 985–995.
Dai, Q., Peng, X., Yang, Z., Zhao, L., 2017. Runoff and erosion processes on bare slopes in the Karst Rocky Desertification Area. Catena 152, 218–226.
Feng, T., Chen, H., Wang, K., Zhang, W., Qi, X., 2014. Modeling soil erosion using a spatially distributed model in a karst catchment of northwest Guangxi, China. Earth Surf. Process. Landf. 39, 2121–2130.
Foster, I.D.L., Lees, J.A., 1999. Changes in the physical and geochemical properties of suspended sediment delivered to the headwaters of LOIS river basins over the last 100 years: a preliminary analysis of lake and reservoir bottom sediments. Hydrol. Process. 13, 1067–1086.
Fu, Z.Y., Chen, H.S., Zhang, W., Xu, Q.X., Wang, S., Wang, K.L., 2015. Subsurface flow in a soil-mantled subtropical dolomite karst slope: a field rainfall simulation study. Geomorphology 250, 1–14.
Gellis, A.C., Walling, D.E., 2011. Sediment source fingerprinting (Tracing) and sediment budgets as tools in Targeting River and watershed restoration programs. Journal of Endovascular Therapy An Official Journal of the International Society of Endovascular Specialists 194, 263–291.
Gennadiev, A.N., Olson, K.R., Chernyanskii, S.S., Jones, R.L., 2002. Quantitative assessment of soil erosion and accumulation processes with the help of a technogenic magnetic tracer. Eurasian Soil Sci. 35, 17–29.
Hartmann, A., Goldscheider, N., Wagener, T., Lange, J., Weiler, M., 2014. Karst water resources in a changing world: review of hydrological modeling approaches. Rev. Geophys. 52, 218–242.
He, Q., Walling, D.E., 1996. Interpreting particle size effects in the adsorption of Cs-137 and unsupported Pb-210 by mineral soils and sediments. J. Environ. Radioact. 30, 117–137.
He, Y., LI, H., Zhang, X., Yan, D., Wen, A., 2009. 137 Cs method study on soil erosion and sediment yield in grass-covered peak cluster depression in Maolan. Guizhou. Carsologica Sinica 28, 181–188.
Herman, J.S., 2012. Water chemistry in caves. In: White, W.B., Culver, D.C. (Eds.), Encyclopedia of Caves (Second Edition). Academic Press, Amsterdam, pp. 881–887.
Herman, E.K., Toran, L., White, W.B., 2012. Clastic sediment transport and storage in fluviokarst aquifers: an essential component of karst hydrogeology. Carbonates Evaporites 27, 211–241.
Jiang, Z., Lian, Y., Qin, X., 2014a. Rocky desertification in Southwest China: impacts, causes, and restoration. Earth. Rev. 132, 1–12.
Jiang, Z., Luo, W., Deng, Y., Cao, J., Qin, X., Li, Y., Yang, Q., 2014b. The leakage of water and soil in the karst peak cluster depression and its prevention and treatment. Acta Geoscientia Sinica 35, 535–542.
Jintao, T.R.X.Z.X., 2004. Grain for Green Project, Grain Policy and Sustainable Development. Soc. Sci. China 6.
Jordanova, D., Jordanova, N., Petrov, P., 2014. Pattern of cumulative soil erosion and redistribution pinpointed through magnetic signature of Chernozem soils. CATENA 120, 46–56.
Li, S., Wu, H., 2015. Mapping karst rocky desertification using Landsat 8 images. Remote. Sens. Lett. 6, 657–666.
Li, Y., Hou, J., Xie, D., 2002. The recent development of research on karst ecology in Southwest China. Scientia Geographica Sinica 22, 363–370.
Li, Z., Xu, X., Liu, M., Li, X., Zhang, R., Wang, K., Xu, C., 2017. State-space prediction of spring discharge in a karst catchment in southwest China. J. Hydrol. (Amst) 549, 264–276.
Li, Z., Xu, X., Zhu, J., Xu, C., Wang, K., 2019. Sediment yield is closely related to lithology and landscape properties in heterogeneous karst watersheds. J. Hydrol. (Amst) 568, 437–446.
Lin, C., Zhu, A., 1999. A study on soil Erosion and prevention in Karst Mountainous Region of Guizhou. Research of Soil and Water Conservation 6, 109–113.
Lu, S., 2003. Chinese Soil Magnetism and Environment. Higher education press.
Mararakanye, N., Sumner, P.D., 2017. Gully erosion: a comparison of contributing factors in two catchments in South Africa. Geomorphology 288, 99–110.
Martin, J.B., Kurz, M.J., Khadka, M.B., 2016. Climate control of decadal-scale increases in apparent ages of eogenetic karst spring water. J. Hydrol. (Amst) 540, 988–1001.
Matisoff, G., Bonniwell, E.C., Whiting, P.J., 2002. Soil erosion and sediment sources in an Ohio watershed using beryllium-7, cesium-137, and lead-210. J. Environ. Qual. 31, 54–61.
Miller, J.R., Mackin, G., Miller, S.M.O., 2015. Application of Geochemical Tracers to Fluvial Sediment.
Ministry of water resources, C.a.o.s., Chinese academy of engineering, 2010. Soil Erosion Control and Ecological Safety in China. Science Press, Beijing.
Nagle, G.N., Ritchie, J.C., 2004. Wheat field erosion rates and channel bottom sediment sources in an intensively cropped northeastern oregon drainage basin. Land Degrad. Dev. 15, 15–26.
Ni, L.S., Fang, N.F., Shi, Z.H., Chen, F.X., Wang, L., 2017. Validating a basic assumption of using CESIUM-137 method to assess soil loss in a small agricultural catchment. Land Degrad. Dev. 28, 1772–1778.
Nosrati, K., Collins, A.L., 2019. Investigating the importance of recreational roads as a sediment source in a mountainous catchment using a fingerprinting procedure with different multivariate statistical techniques and a Bayesian un-mixing model. J. Hydrol. (Amst) 569, 506–518.
Olson, K.R., Gennadiyev, A.N., Jones, R.L., Chernyanskii, S., 2002. Erosion patterns on cultivated and reforested hillslopes in Moscow region. Russia. Soil Sci. Soc. Am. J. 66, 193–201.
Owens, P.N., Blake, W.H., Gaspar, L., Gateuille, D., Koiter, A.J., Lobb, D.A., Petticrew, E.L., Reiffarth, D.G., Smith, H.G., Woodward, J.C., 2016. Fingerprinting and tracing the sources of soils and sediments: earth and ocean science, geoarchaeological, forensic, and human health applications. Earth. Rev. 162, 1–23.
Palazón, L., Latorre, B., Gaspar, L., Blake, W.H., Smith, H.G., Navas, A., 2015. Comparing catchment sediment fingerprinting procedures using an auto-evaluation approach with virtual sample mixtures. Sci. Total Environ. 532, 456–466.
Peng, T., Wang, S.J., 2012. Effects of land use, land cover and rainfall regimes on the surface runoff and soil loss on karst slopes in southwest China. Catena 90, 53–62.
Peng, T., Wang, S., Zhang, X., Rong, L., Yang, T., Chen, B., Wang, J., 2008. Results of preliminary monitoring of surface runoff COEFFICIENTS FOR KARST SLOPES. Earth and Environment 36, 125–129.
Peng, J., Xu, Y.Q., Cai, Y.L., Xiao, H.L., 2011. The role of policies in land use/cover change since the 1970s in ecologically fragile karst areas of Southwest China: a case study on the Maotiaohe watershed. Environ. Sci. Policy 14, 408–418.
Peng, J., Xu, Y.Q., Zhang, R., Xiong, K.N., Lan, A.J., 2013. Soil erosion monitoring and its implication in a limestone land suffering from rocky desertification in the Huajiang Canyon, Guizhou, Southwest China. Environ. Earth Sci. 69, 831–841.
Poesen, J., Nachtergaele, J., Verstraeten, G., Valentin, C., 2003. Gully erosion and environmental change: importance and research needs. Catena 50, 91–133.
Pulley, S., Collins, A.L., 2018. Tracing catchment fine sediment sources using the new SIFT (SedIment Fingerprinting Tool) open source software. Sci. Total Environ. 635, 838–858.
Rahimi, M.R., Ayoubi, S., Abdi, M.R., 2013. Magnetic susceptibility and Cs-137 inventory variability as influenced by land use change and slope positions in a hilly, semiarid region of west-central Iran. J. Appl. Geophy. 89, 68–75.
Rousseeuw, P.J., Croux, C., 1993. Alternatives to the median absolute deviation. J. Am. Stat. Assoc. 88, 1273–1283.
Russell, M.A., Walling, D.E., Hodgkinson, R.A., 2001. Suspended sediment sources in two small lowland agricultural catchments in the UK. J. Hydrol. (Amst) 252, 1–24.
Sadiki, A., Faleh, A., Navas, A., Bouhlassa, S., 2009. Using magnetic susceptibility to assess soil degradation in the Eastern Rif, Morocco. Earth Surf. Process. Landf. 34, 2057–2069.
Theuring, P., Collins, A.L., Rode, M., 2015. Source identification of fine-grained suspended sediment in the Kharaa River basin, northern Mongolia. Sci. Total Environ. 526, 77–87.
Wan, G., Lin, W., Huang, R., Chen, Z., 1991. Dating characteristics and erosion traces of 137Cs vertical profiles in Hongfeng Lake sediments. Chinese Sci. Bull. 36 674-674.
Wang, F., Li, R., Yang, Q., 2003. Review on effects of human activities on the soil Erosion in the Loess Plateau. J. Sediment. Res. A Sediment. Petrol. Process. 0, 74–80.
Wang, J., Zou, B., Liu, Y., Tang, Y., Zhang, X., Yang, P., 2014. Erosion-creep-collapse mechanism of underground soil loss for the karst rocky desertification in Chenqi village, Puding county, Guizhou, China. Environ. Earth Sci. 72, 2751–2764.

Wei, X., 2013. Monitoring of soil erosion and nutrient loss on the mountain slope in karst valley region based on isotope. Transactions of the Chinese Society of Agricultural Engineering 29, 128–136.
Wei, X., Yan, Y., Xie, D., Ni, J., Loaiciga, H.A., 2016. The soil leakage ratio in the Mudu watershed, China. Environ. Earth Sci. 75.
Wenbo, W., Yunlong, C.A.I., Hongya, W., 2008. Dating by sediment grain size and ~(137)Cs in small reservoir:a case study of Kechou reservoir,in Karst area of central Guizhou Province. Scientia Limnologica Sinica 20, 306–314.
White, W.B., 2007. Brief history of karst hydrogeology: contributions of the NSS. J. Karst Stud. 69, 13–26.
Wilcox, B.P., Wilding, L.P., Woodruff, C.M., 2007. Soil and topographic controls on runoff generation from stepped landforms in the Edwards Plateau of Central Texas. Geophys. Res. Lett. 34, 6.
Williams, P.W., 1983. The role of the subcutaneous zone in karst hydrology. J. Hydrol. (Amst) 61, 45–67.
Yuan, D., 1997. Rock desertification in the subtropical karst of south China. Zeitschrift fur Geomorphologie 108.
Zhang, X., Wang, S., He, X., Wang, Y., He, Y., 2007. Soil creeping in weathering crusts of carbonate rocks and underground soil losses on KARST SLOPES. Earth and Environment 35, 202–206.
Zhang, X.-N., Wang, K.-L., Zhang, W., Chen, H.-S., He, X.-Y., Zhang, X.-B., 2009. Distribution of 137Cs and relative influencing factors on typical karst sloping land. Huan Jing Ke Xue 30, 3152–3158.
Zhang, X., Wang, S., Cao, J., Wang, K., Meng, T., Bai, X., 2010. Characteristics of water loss and soil erosion and some scientific problems on karst rocky desertification in Southwest China karst area. Carsologica Sinica 29, 274–279.
Zhang, X., Bai, X., Liu, X., 2011. Application of a Cs-137 fingerprinting technique for interpreting responses of sediment deposition of a karst depression to deforestation in the Guizhou Plateau, China. Science China-Earth Sciences 54, 431–437.
Zhang, Z.C., Chen, X., Huang, Y.Y., Zhang, Y.F., 2014. Effect of catchment properties on runoff coefficient in a karst area of southwest China. Hydrol. Process. 28, 3691–3702.
Zhao, G., Klik, A., Mu, X., Wang, F., Gao, P., Sun, W., 2015. Sediment yield estimation in a small watershed on the northern Loess Plateau, China. Geomorphology Amst. (Amst) 241, 343–352.
Zhao, G., Mu, X., Han, M., An, Z., Gao, P., Sun, W., Xu, W., 2017. Sediment yield and sources in dam-controlled watersheds on the northern Loess Plateau. CATENA 149, 110–119.
Zhou, J., Tang, Y., Yang, P., Zhang, X., Zhou, N., Wang, J., 2012. Inference of creep mechanism in underground soil loss of karst conduits I. Conceptual model. Nat. Hazards 62, 1191–1215.